

A Comprehensive Study of Gamma-Ray Burst Optical Emission: III. Brightness Distributions and Luminosity Functions of Optical Afterglows

Xiang-Gao Wang¹, En-Wei Liang^{1,2}, Liang Li¹, Rui-Jing Lu¹, Jian-Yan Wei², Bing Zhang^{3,1}

ABSTRACT

We continue our systematic statistical study on optical afterglow data of gamma-ray bursts (GRBs). We present the apparent magnitude distributions of early optical afterglows at different epochs ($t = 10^2$ s, $t = 10^3$ s, and 1 hour) for the optical lightcurves of a sample of 93 GRBs (the global sample), and for sub-samples with an afterglow onset bump or a shallow decay segment. For the onset sample and shallow decay sample we also present the brightness distribution at the peak time t_p and break time t_b , respectively. All the distributions can be fit with Gaussian functions. We further perform Monte Carlo simulations to infer the luminosity function of GRB optical emission at the rest-frame time 10^3 seconds, t_p , and t_b , respectively. Our results show that a single power-law luminosity function is adequate to model the data, with indices -1.40 ± 0.10 , -1.06 ± 0.16 , and -1.54 ± 0.22 , respectively. Based on the derived rest-frame 10^3 s luminosity function, we generate the intrinsic distribution of the R-band apparent magnitude M_R at the observed time 10^3 seconds post trigger, which peaks at $M_R = 22.5$ mag. The fraction of GRBs whose R-band magnitude is fainter than 22 mag, and 25 mag and at the observer time 10^3 seconds are $\sim 63\%$ and $\sim 25\%$, respectively. The detection probabilities of the optical afterglows with ground-based robotic telescopes and UVOT onboard *Swift* are roughly consistent with that inferred from this intrinsic M_R distribution, indicating that the variations of the dark GRB fraction among the samples with different telescopes may be due to the observational selection effect, although the existence of an intrinsically dark GRB population cannot be ruled out.

Subject headings: radiation mechanisms: non-thermal — gamma-rays: bursts — method: statistics

¹Department of Physics and GXU-NAOC Center for Astrophysics and Space Sciences, Guangxi University, Nanning 530004, China;lew@gxu.edu.cn

²National Astronomical Observatories, Chinese Academy of Sciences, Beijing, 100012, China

³Department of Physics and Astronomy, University of Nevada, Las Vegas, NV 89154, USA

1. Introduction

Optical afterglows have been detected from ~ 250 gamma-ray bursts (GRBs) since the first optical counterpart was identified in February 28, 1997 (van Paradijs et al. 1997). The observed magnitudes span from 5.5 to 28 mag, in a time-window from tens to 10^7 seconds past the GRB trigger, with telescopes whose apertures range from tens of centimeters to 10 meters. Statistical studies of optical afterglow lightcurves have been carried out by some authors and some general features of the lightcurves have been reported. For example, optical lightcurves have been compiled in the rest frame of GRBs, and two universal tracks have been claimed (Liang & Zhang 2006; Nardini et al. 2006; Kann et al. 2006. c.f., Melandri et al. 2008, Oates et al., 2009, Zaninoni et al 2013). Panaitescu & Vestrand (2008, 2011) showed some general features of the early bumps and plateaus in the optical lightcurves. Akelof & Swan (2007) estimated the apparent optical brightness distribution function and suggested that the apparent optical magnitude distribution peaks at $R \sim 19.5$. Kann et al. (2010, 2011) compared the optical lightcurves of two types of GRBs. We carry out a systematical analysis of the optical data of GRBs and present our results in a series of papers. In the first two papers of this series (Li et al. 2012, paper I; Liang et al. 2012, paper II), we presented general features of a “synthetic” optical lightcurve based on our decomposition analysis of lightcurves, and focused on the statistical properties and the physical implications of the optical flares, the shallow decay segment, the afterglow onset bump, and the late re-brightening component. We showed that the optical flares and the shallow decay segment may signal late central engine activity (Paper I), and that the onset bumps and late re-brightening bumps may probe the properties of the fireball and its surrounding medium density (Paper II; see also Rykoff et al.2009; Oates et al. 2009; Liang et al. 2010; Lü et al. 2012; Ghirlanda et al. 2012; Yi et al. 2012).

The luminosity function of GRB afterglows is poorly known since no complete sample in a given threshold is available. Observationally, the detection of an optical counterpart of a GRB depends on the instrument, exposure time, observation epoch, etc. For example, the UV-optical telescope (UVOT) on board *Swift* promptly slews to the GRB trigger positions, and $\sim 27\%$ of GRBs were detected at the 3σ level (in an individual exposure; Roming et al. 2009), but $\sim 60\%$ of all GRBs have been detected by ground-based telescopes in the spectral bands redder than UVOT (e.g., Akelof & Swan 2007 using GCN data). The optical afterglows may also suffer significant dust extinction by the host galaxies of GRBs, since long GRBs are believed to be born in dusty, opaque star-forming regions (Reichart & Price 2002; Kloise et al. 2003; Vergani et al. 2004; Levan et al. 2006). They are not visible at all in the optical band due to the Lyman- α absorption of neutral hydrogen, if a GRB originates at a high redshift (Jakobsson et al. 2004; 2005). In addition, the observed optical emission may be the superposition of multiple components with distinct physical origins, whose strengths

and decay slopes may vary from burst to burst (e.g., Li et al. 2012). These effects cause complications in revealing the luminosity function of optical afterglows.

This paper continues our systematic statistical study on optical afterglow data. We study a sample of 93 GRBs with optical detections before $t < 1$ hour (the global sample), and two sub-samples whose lightcurves show an onset bump or a shallow decay segment, respectively (see e.g. Paper I and II). For these three samples, we present the apparent R-band magnitude distributions of early optical afterglows at several different epochs ($t = 10^2$ s, $t = 10^3$ s and 1 h) after the triggers. We then use Monte Carlo simulations to investigate the intrinsic luminosity function of the GRB optical afterglows at the rest-frame $t = 10^3$ s, at the peak time t_p for the sample that show an onset bump in the lightcurves, and at the break time t_b for the sample that show a shallow decay segment. The early optical lightcurves are rich in features that may be attributed to different physical origins. A significant fraction of the lightcurves are dominated by a clear onset bump that signals the deceleration of the fireball, which is most sensitively defined by the fireball initial Lorentz factor (Paper II). Some others show a shallow decay segment, which is related continuous energy injection into the blastwave (Paper I). The end time of this phase t_b is related to a critical time of late energy injection from the GRB central engine or related to a critical time when pile-up of flare materials onto the blastwave is over. We therefore also study the luminosity functions at t_p and t_b , which may hold the key in studying the fireball parameters and the late central engine activities. We describe our samples in §2. The observed R-band magnitude distributions at various epochs are presented in §3. A Monte Carlo simulation analysis is presented in §4 to infer the optical luminosity function at rest-frame $t = 10^3$ s, t_p and t_b . Conclusions and discussion are presented in §5.

2. Sample and Data

We have compiled a large sample of GRB optical data from published papers or from GCN Circulars when no published paper is available. Well-sampled lightcurves are available for 146 GRBs, as shown in Figure 1. Galactic extinction correction is made to the data by using a reddening map presented by Schlegel et al. (1998). Most data are in the R-band. Those data that were obtained in other wavelengths are corrected to the R band with the optical spectral indices (β_O) collected from the literature ¹. These lightcurves were

¹The convention $F_\nu \propto \nu^{-\beta_O}$ is used. An optical spectral index $\beta_O = 0.75$ is adopted for those GRBs whose β_O is not available. The extinction A_V of the host galaxy and the spectral index of the optical afterglow for each burst from the same literature is also used to reduce the uncertainties introduced by different authors.

decomposed into multiple empirical components with smooth broken power-law functions. The details of the fitting results are reported in Papers I and II. From 146 GRBs, we focus on early optical afterglows and select 93 GRBs that have optical detections at $t < 1$ hour. This is our *global* sample. We calculate the brightness at $t = 10^2, 10^3$ seconds and 1 hour for this sample using empirical fits to the lightcurves. The redshift, temporal coverage of the lightcurve data, and the derived brightness in these epochs are reported in Table 1. A sub-sample of 39 GRBs have a smooth afterglow onset bump in the lightcurve, and a sub-sample of 26 GRBs have a shallow decay segment in the lightcurves (Liang et al. 2012). We also derive the brightness at $t = 10^2, 10^3$ seconds and 1 hour for these two sub-samples based on our empirical fits available in Papers I and II. The brightness at the peak time (t_p) of the afterglow onset bumps and the end time (t_b) of the shallow decay segments are also calculated with the results of the empirical fits. They are reported in Tables 2 and 3.

Note that the current deepest survey for early optical afterglows is made with the GROND telescope (Greiner et al. 2011). It has a limit of $M_R \sim 25$ mag. As shown in Figure 1, we do not find GRBs that have detections dimmer than 22 mag at $t < 10^2$ seconds in our sample. We check the observations with the GROND telescope for $t < 10^3$ seconds and found that some GRBs have been detected with $R > 22$ mag for a few cases (such as GRB 081029, $R=22.8$ at 240 s, GCN 7231; GRB 081029, $R \sim 24.3$ at 660s, GCN 8731). Our sample includes only the GRBs that have well-sampled lightcurves. Therefore, the non-detection with $M_R > 22$ mag at 10^3 seconds in our sample is due to the sample selection effect. This selection effect, however, does not impact on our analysis results since we perform simulations with a limit of $M_R = 19$ mag (see §4.2).

3. Apparent Magnitude Distributions

Among the 93 GRBs in our sample, 89 GRBs have optical detections earlier than 10^3 s, and 36 GRBs have optical detections earlier than $t = 10^2$ seconds. We obtain the luminosity at $t=10^2$ seconds for the 36 GRBs from our empirical fits. We also derive the luminosity at $t=10^2$ for the other GRBs that have optical detection earlier than 10^3 seconds (most of them have detection very closed to 10^2 seconds, see Figure 1) by extrapolating our empirical fits to $t=10^2$ seconds. The lightcurves of 7 GRBs are poorly sampled or rapidly increase between 10^2 and 10^3 seconds. We do not derive the luminosity at $t=10^2$ from these lightcurves. We therefore finally obtain a sample of 82 GRBs that have optical luminosity at $t=10^2$ seconds. Figure 2 shows the distributions of the apparent magnitudes at $t = 10^2, 10^3$ seconds and 1 hour post the GRB triggers for the global lightcurves. The distributions at $t = 10^2$ and 10^3 seconds are well fit with a Gaussian function, and the derived central values with 1σ

deviations are $M_{R,c} = 16.1 \pm 1.8$ mag and 17.3 ± 1.8 mag (1σ), respectively. The magnitudes at $t = 1$ hour of the 93 GRBs are narrowly distributed in the range $M_R = 14 - 22$ mag, with a Gaussian fit of $M_{R,c} = 18.4 \pm 1.6$ mag. The fact that these distributions can be fitted with Gaussian without a sharp cut-off at the low flux end may be due to the fact that the current sample was obtained from observations of telescopes with different flux limits.

A smooth onset hump is observed in 39 GRBs in our sample. We show the brightness distributions for this component at $t = 10^2, 10^3$ seconds, 1 hour and at $t = t_p$. In general, they are roughly consistent with that for the global lightcurves as shown in Figure 2. The brightness distribution at $t = t_p$ is well fit with a broad Gaussian function, i.e., $M_{R,c} = 15.6 \pm 2.2$ mag, with 95% having $M_R < 19$. This may be due to the observational selection effect since the onset bump is usually detected using small aperture telescopes in a moderate limit of $M_R \sim 19$ mag.

The standard fireball model suggests that the decay slope of the afterglows should be steeper than 0.75 if no additional energy is continuously injected into the blastwave. Liang et al. (2012) defined a shallow decay segment with the criterion that the decay slope is initially shallower than 0.75, which transits to a steeper decay after a break time t_b . Such a segment is observed in 26 GRBs in our GRB sample. We also show the brightness distributions for this component at $t = 10^2, 10^3$ seconds, 1 hour and at $t = t_b$ in Figure 2. They are also roughly consistent with those for the global sample. This is reasonable since the early optical lightcurves are usually dominated by the onset bump or the shallow decay segment. The brightness at t_b is $M_{R,c} = 18.3$ mag.

4. CONSTRAINING THE INTRINSIC LUMINOSITY FUNCTIONS WITH MC SIMULATIONS

The luminosity of a GRB afterglow at a given time depends on the kinetic energy, micro-physical parameters and radiation efficiency of the fireball (e.g., Sari et al. 1998). No universal values for these quantities are found among bursts, and the correlation between the luminosities of the prompt gamma-rays and the optical afterglow is loose. One cannot simply infer the optical luminosity function from that of the prompt gamma-ray emission. Here we take optical afterglow as independent of their γ -ray luminosity function, and perform Monte Carlo simulations. Since the optical luminosity depends on the epoch, in the following we constrain the luminosity function at 10^3 s after the GRB trigger in the rest frame of GRBs. In order to study the deceleration physics and energy injection physics, we also constrain the luminosity functions at t_p and t_b , respectively. Since these times differ from burst to burst, there is no need to differentiate the rest-frame and the observer-frame.

4.1. Model

The number density of GRBs at redshift $z \sim z + dz$ is given by

$$n(z) = \frac{dN}{dz} = \frac{R_{\text{GRB}}(z)}{1+z} \frac{dV(z)}{dz}, \quad (1)$$

where $R_{\text{GRB}}(z)$ is the co-moving GRB rate as a function of z , the factor $(1+z)^{-1}$ accounts for the cosmological time dilation of the observed rate, and $dV(z)/dz$ is the co-moving volume element. We assume R_{GRB} traces the star formation rate and metallicity history, e.g. (Kistler et al. 2008; Li 2008; Qin et al. 2010; Virgili et al. 2011; Lu et al. 2012)

$$R_{\text{GRB}}(z) = \rho_0 R_{\text{SFR}}(z) (1+z)^\delta \Theta(\epsilon, z), \quad (2)$$

where ρ_0 is the local GRB rate in units of $\text{Gpc}^{-3} \text{ yr}^{-1}$, $(1+z)^\delta$ accounts for the possible GRB rate evolution effect in excess of the SFR rate, $\Theta(\epsilon, z)$ is the fractional mass density belonging to the metallicity below ϵZ_\odot at a given z (Z_\odot is the solar metal abundance), and ϵ is determined by the metallicity threshold for the production of GRBs. The star-forming rate $R_{\text{SFR}}(z)$ is taken as (Langer & Norman 2006; Kistler et al. 2008),

$$R_{\text{SFR}}(z) \propto \begin{cases} (1+z)^{3.44}, & z \leq 1 \\ (1+z_{\text{peak}})^{3.44}, & z > 1 \end{cases}. \quad (3)$$

The $\Theta(\epsilon, z)$ is parameterized as (Hopkins & Beacom 2006; Langer & Norman 2006)

$$\Theta(\epsilon, z) = \frac{\hat{\Gamma}(\hat{\alpha} + 2, \epsilon^{\hat{\beta}} 10^{0.15 \hat{\beta} z})}{\Gamma(\hat{\alpha} + 2)}, \quad (4)$$

where $\hat{\alpha}$ and $\hat{\beta}$ are the lower and higher end indices of the galaxy mass - metallicity relation, and $\hat{\Gamma}(a, x)$ and $\Gamma(x)$ are the incomplete and complete gamma function (Langer & Norman 2006; Kistler et al. 2008), respectively. We take $\alpha_\gamma = -1.16$, $\beta_\gamma = -2$, $\epsilon = 0.4$, and $\delta = 0.4$ (Qin et al. 2010)².

Assuming the optical spectrum as $F_\nu \propto \nu^{-\beta_0}$, the observed flux by considering the k-correction effect would be

$$F_\nu = \frac{L_\nu(\nu_0)(1+z)^{1-\beta_0}}{4\pi D_L^2(z)}, \quad (5)$$

²As discussed in Qin et al. (2010), the metallicity factor may vary from 0.2 to 0.6 derived from Monte Carlo simulations for the GRB rate. Being due to small samples in our analysis, we find that the variation of the fraction from 0.2 to 0.6 does not significantly change our results.

where $D_L(z)$ is the luminosity distance at z , ν_0 is the frequency in the burst frame. The observed R-band magnitude by considering dust extinction in the GRB host galaxy (A_V^{host}) is

$$M_R = \frac{\log(F_R/F_{R,0})}{-0.4} + A_V^{\text{host}}, \quad (6)$$

where $F_{R,0} = 1.218 \times 10^{-5}$ erg cm $^{-2}$ s $^{-1}$. Here we take the central frequency and the full-width-half-maximum of the R band as 7000Å and 2200Å, respectively. We assume that the optical afterglows are the synchrotron radiation in the spectral regime $\nu_m < \nu < \nu_c$, and take $\beta_O = 0.75$ for an electron power-law index $p = 2.3$.

4.2. Simulation procedure and results

We assume that the luminosity functions of GRB optical afterglow at rest-frame $t = 10^3$ s post trigger, at t_p and t_b can be all characterized as a single power-law or a smooth broken power-law³

$$\Phi(L) = \Phi_0(L/L_0)^\alpha \quad (7)$$

$$\Phi(L) = \Phi_0\left[\left(\frac{L}{L_b}\right)^{\alpha_1} + \left(\frac{L}{L_b}\right)^{\alpha_2}\right]^{-1}, \quad (8)$$

where Φ_0 is a normalization constant and L_0 is taken as 10^{46} erg/s. We use the optical afterglow data to constrain the luminosity function parameters by Monte Carlo simulations in the luminosity range of $[10^{43}, 10^{50}]$ erg s $^{-1}$. The details of our simulation procedure are as follows.

(1) Generate a redshift and a luminosity for the optical afterglow from the probability distributions of the redshift and luminosity based on Eqs. 1 and 7 (or 8) with a set of free parameters, respectively. We take a redshift range of $[0, 6.3]^4$ and a luminosity range of $[10^{43}, 10^{50}]$ erg s $^{-1}$.

(2) Calculate the observed apparent magnitude of the simulated GRB with Eqs. (5) and (6). The A_V value is generated from the A_V distribution of current sample with A_V available, which is shown in Table 4 and Figure 3. The distribution of A_V can be fitted with a log-normal function, i.e., $\log(A_V) = -0.63 \pm 0.42(1\sigma)$.

³It is known that the GRB luminosity function can be characterized with a broken power-law or a cut-off power-law (e.g., Schmidt 2001; Zhang et al. 2004; Guetta et al. 2005; Liang et al. 2007). Therefore, we try to use the same function form to describe the optical afterglow luminosity function.

⁴The observed R-band emission would be significantly affected by the Lyman- α absorption for a GRB at $z > 6$. We therefore take an upper limit of the redshift as that of GRB 050904, i.e., $z = 6.3$.

(3) Compare the mock sample with the observations in the $\log M_R - \log(1+z)$ plane. To constrain the 10^3 s luminosity function, for the observational data we identify the relevant epoch in the observer frame to make sure that it corresponds to the rest-frame 10^3 s post trigger. The observed sample suffers observational biases. The optical data in the current sample are collected from observations with different telescopes. The optical telescopes do not have a clean flux limit as high energy instruments. The early optical data are usually observed with robotic telescopes with small apertures. The flux limit of these telescope is usually 19 mag. We therefore compare the mock sample with the observed sample by screening the samples with a threshold of $M_R = 19$ mag. We evaluate the consistency of the z and M_R distributions between the mock and observed samples with a Kolmogorov-Smirnov test (K-S test). Note that the magnitude of a simulated GRB is derived from the luminosity and redshift. To compare a simulated GRB sample with observations, the GRB sample is screened by the instrumental threshold. The magnitude of a GRB with larger luminosity at higher redshift may be the same as a GRB with smaller luminosity at lower redshift. Therefore, the consistency of the magnitude distributions between the simulated and observed samples alone cannot ensure the consistency between the redshift distributions. Therefore, we define a global probability of the K-S test (P_{K-S}^G) to measure the consistency of both the magnitude and redshift distributions between the simulated and observed sample as $P_{K-S}^G = P_{K-S}^M \times P_{K-S}^z$, where P_{K-S}^M and P_{K-S}^z are the probabilities of the K-S tests for the M_R and z distributions, respectively. A larger value of P_{K-S} indicates a better consistency. Generally, a value of $P_{K-S} > 0.1$ is acceptable to claim statistical consistency, whereas a value of $P_{K-S} < 10^{-4}$ convincingly rejects the consistency hypothesis.

We repeat the above steps to search for the best consistency in a broad parameter space. In our simulations, a mock GRB is characterized with a set of $\{z, L, A_V\}$. We generate a sample of 10^5 mock GRBs based on a luminosity function with a given power-law index α (or a set of $\{\alpha_1, \alpha_2\}$ for a broken luminosity function). We then measure the consistency between the mock GRB sample and the observed sample with the K-S test. We make 10^5 trials for α (or $\{\alpha_1, \alpha_2\}$ for a broken luminosity function) randomly in the range of $[0, -2.5]$ and show P_{K-S}^G as a function of α to find the α value that gives the best consistency between the simulations and observations. We evaluate the luminosity function of the global lightcurves at $t = 10^3$ seconds. The selection of this specified epoch is due to that both ground-based and spaced-based telescopes with different apertures may make observations at this epoch. We also estimate the luminosity functions at the afterglow onset peak and at the break time of the shallow decay segments. We find that the constraints on the parameters of a broken power-law luminosity function with the current sample is loose, and a single power-law luminosity function is adequate to model the current sample. The P_{K-S}^G distributions for different α values is shown in Figure 4. The Gaussian fits yield $\alpha = -1.40 \pm 0.10$,

-1.06 ± 0.16 , and -1.54 ± 0.22 for the luminosity functions at rest-frame $t = 10^3$ seconds of the global-sample lightcurves, at the peak time t_p of the onset bumps, and at the break time t_b of the shallow decay segments, respectively. The errors are in 1σ confidence level. We also randomly generate a sub-sample that has the same size as the observed sample based on a luminosity function with $\alpha = -1.40 \pm 0.10$. Figures 5-7 demonstrates the consistency between the simulated and observational samples in the 2-dimensional $M_R - \log(1 + z)$ plane and in the 1 dimensional M_R and $\log(1 + z)$ distributions. One can observe that the luminosity functions can produce the observational data. The slope of the luminosity functions for the global sample lightcurves and that of the shallow decay segment break time t_b are consistent. This would be due to the fact that t_b is usually at several hundreds to several thousands of seconds with a typical value of $\sim 10^3$ seconds (Li et al. 2012). The slope of the luminosity function at the onset bump t_p is shallower than that derived at t_b .

Based on the derived luminosity function, we generate the intrinsic distribution of M_R at the observed 10^3 seconds for the global sample. We generate a sample of 10^5 GRBs in the luminosity range $[10^{43} \sim 10^{50}]$ erg/s based on the rest-frame luminosity function with $\alpha = -1.40 \pm 0.10$. Fixing the model parameters of the GRB rate (Eq. 2), we calculate the M_R values of the mock GRBs at the observed 10^3 s post-trigger. To do so, we extrapolated lightcurves from the rest-frame 10^3 s to the observer-frame 10^3 s by introducing a decay slope for each lightcurve, the distribution of which is derived from the observed decay-slope distribution. The resulting observer-frame 10^3 s M_R distribution is shown in Figure 8. The accumulated probability distribution of M_R is also shown. The peak of the distribution is $M_R = 22.5$ mag, which is dimmer by 3 mag than the peak of the apparent optical magnitude distribution ($M_R \sim 19.5$) reported by Akelof & Swan (2007). This would be due to observational selection effect in the sample used by Akelof & Swan (2007).

We examine the detection probability for GRB optical afterglow surveys using telescopes with different flux limits. Small aperture robotic telescopes for early optical afterglow observations, such as ROTSE (Akerlof et al. 2003) and KAIT (Filippenko et al. 2001), usually have a limit of $M_R \sim 18 - 19$ mag. As shown in Figure 8, with this limit the fraction of the optical afterglows that can be detectable is only $\sim 19\%$. We check the detection probability with ROTSE⁵ and find that this fraction is 27/89 for the ROTSE responses earlier than 10^3 seconds post the GRB triggers. The slight difference between our prediction and the ROTSE observations may be due to the fact that the ROTSE responses are usually much earlier than 10^3 s post the GRB triggers. The current largest robotic optical telescopes for GRB optical afterglow survey are the Liverpool and Faulkes Telescopes (North and South). They have a

⁵http://www.rotse.net/grb_reports/

limit of ~ 22 mag. The detection fraction with these telescopes is 24/63 in the first 10 minutes. This fractions are consistent with that derived from Figure 8 with a limit of $M_R = 22$ mag, i.e., 37%. The UV-optical telescope (UVOT) on board *Swift*, which has a limit of ~ 20 mag, promptly slewed to the GRB trigger positions and detects $\sim 27\%$ of GRBs at the 3σ level (in an individual exposure)⁶. The fraction of UVOT detection is consistent with our result shown in Figure 8. Note that, the detection probability with the Palomar 60 inch telescope, which is a robotic telescope with a response time of ~ 180 seconds and a limiting magnitude of $M_R = 20.5$ (Cenko et al. 2006), is 22/29 from a sample made during 2005-2008 (Cenko et al. 2009). The high detection efficiency may be due to the fact that P60 has a redder coverage than UVOT. The detection efficiency of GROND, a simultaneous 7-channel optical/near-infrared imager (Greiner et al. 2008) mounted at the 2.2m MPI/ESO telescope with a detection limit of $M_R \sim 25.3$ mag, is even higher, which is $\sim 91\%$ and $\sim 88\%$ within 0.5 hours and 0.5 \sim 4 hours after the trigger, respectively (Greiner et al. 2011). The fraction of GRBs with $M_R = 25.3$ mag derived from Figure 8 is 77%, which is slightly lower than the detection probability with GROND. This would be also due to redder coverage of GROND.

5. CONCLUSIONS AND DISCUSSION

We have presented the brightness distributions of early optical afterglows at different epochs derived from the empirical fits to the observed lightcurves for a sample of 93 GRBs that have optical detection at $t < 1$ hour post the GRB triggers. The typical R-band flux at $t = 10^2$ s, 10^3 s, and 1 hour are 16.1, 17.1, and 18.4 mag, respectively, for the all sample. We also derive the distributions at these epochs for the sub-samples that show an afterglow onset bump feature and the shallow decay segment. They are generally consistent with that derived from the global sample. The brightness at the peak time of the bumps falls in the range of $R = 9 \sim 22$ mag, with a typical value of $M_R = 15.6$ mag. The typical brightness at the break time of the shallow decay segment is $M_R = 18.3$ mag.

We further perform Monte Carlo simulations to study the luminosity functions of the optical afterglows for the global sample at the rest-frame 10^3 seconds, for the afterglow onset bumps at t_p , and for the shallow decay segment at t_b . We find that a single power-law luminosity function is adequate to describe the data, with the indices -1.40 ± 0.10 , -1.06 ± 0.10 , and -1.54 ± 0.22 for the three samples, respectively. Based on the derived luminosity function, we generate the intrinsic distribution of M_R at 10^3 seconds and show

⁶Note that the fraction of UV-optical counterpart detection with UVOT for Swift GRBs varies for the epoch selection and the limit from one exposure or co-add more exposure (Roming et al. 2006; 2009).

that the distribution peaks at $M_R = 22.5$ mag. The detection probabilities of the optical afterglows with ground-based robotic telescopes and UVOT onboard *Swift* are consistent with our results.

The nature of optically dark GRBs is still not fully uncovered. The proposed explanations for the dark GRBs are essentially classified into two classes: extrinsic and intrinsic effects. The extrinsic effects include extinction and/or absorption by the host galaxies, foreground extinction, Lyman- α absorption, etc. The intrinsic effects include intrinsic faintness or rapidly decay of the optical afterglow due to a low-density environment, and suppression of reverse shock optical emission in a Poynting-flux dominated jet, etc (Zhang 2007 and references therein). Some authors quantified the degree of optical darkness with the upper limit on the afterglow flux (Rol et al. 2005) or with the optical-to-X-ray spectral index (Jakobsson et al. 2004). Note that the fraction of GRBs with no optical detection is dramatically different among samples, ranging from 20% to 60% (Melandri et al. 2008, 2012; Cenko et al. 2009; Zheng et al. 2009; Gehrels et al. 2008; Fynbo et al. 2009 and Greiner et al. 2011). The non-detection of an optical counterpart in these samples should be partially due to observation selection effects. For example, about $\sim 27\%$ of *Swift* GRBs were detected with UVOT at the 3σ level (in an individual exposure; Roming et al. 2009), but $\sim 60\%$ were detected by ground-based telescopes in redder bands than the UVOT bands. Although we cannot exclude the existence of an intrinsically optically dark GRB population, the intrinsic M_R distribution derived from our luminosity functions at $t = 10^3$ seconds may, at least partially, account for the non-detection of an optical counterpart in some GRBs. As discussed in §2, the non-detection of optical afterglows dimmer than 22 mag at $t = 10^3$ seconds in our sample would be due to the observational selection effect. From Figure 1, one can see that the fraction of GRBs with optical afterglows dimmer than 22 at this epoch is $\sim 63\%$. Even with a deep limit of $M_R = 25$ mag, this fraction is still $\sim 25\%$. Therefore, the variation of the fractions of optically dark GRBs may be partially due to the sample selection effect.

The Visible Telescope (VT) on board the upcoming Space-based Variable Objects Monitor (SVOM), a new Chinese-French mission aiming at studying GRBs, has a limiting magnitude of 23 mag (5σ significance level) for a 300 s exposure time (Paul et al. 2011). The fraction of GRBs that would be detectable with VT inferred from our result is 56% at $t = 10^3$ seconds. As shown in Figure 2, the optical afterglows at $t = 10^2$ seconds are brighter than that at 10^3 seconds by about one magnitude. The rapid slewing capacity of VT may further increase this fraction at an earlier epoch. Such a sensitivity is a significant improvement over the UVOT for the GRB early optical afterglow study.

This work is supported by the National Basic Research Program (973 Programme) of China (Grant 2009CB824800), the National Natural Science Foundation of China (Grants

11025313, 11163001, 11203008), Special Foundation for Distinguished Expert Program of Guangxi, and the Guangxi Natural Science Foundation (2013GXNSFFA019001, 2010GXNSFA013112, 2010GXNSFC013011, and Contract No. 2011-135). BZ acknowledges support from NSF (AST-0908362).

REFERENCES

- Akerlof, C. W., & Swan, H. F. 2007, *ApJ*, 671, 1868
- Berger, E., Chary, R., Cowie, L. L., et al. 2007, *ApJ*, 665, 102
- Cano, Z., Bersier, D., Guidorzi, C., et al. 2011, *MNRAS*, 413, 669
- Castro-Tirado, A. J., Jelínek, M., Pandey, S. B., et al. 2006, *A&A*, 459, 763
- Cenko, S. B., Kelemen, J., Harrison, F. A., et al. 2009, *ApJ*, 693, 1484
- de Ugarte Postigo, A., Fatkhullin, T. A., Jóhannesson, G., et al. 2007, *A&A*, 462, L57
- de Ugarte Postigo, A., Horváth, I., Veres, P., et al. 2011, *A&A*, 525, A109
- Ferrero, P., Klose, S., Kann, D. A., et al. 2009, *A&A*, 497, 729
- Filippenko, A. V., Li, W. D., Treffers, R. R., & Modjaz, M. 2001, *IAU Colloq. 183: Small Telescope Astronomy on Global Scales*, 246, 121
- Fynbo, J. P. U., Jakobsson, P., Prochaska, J. X., et al. 2009, *ApJS*, 185, 526
- Götz, D., Covino, S., Hascoët, R., et al. 2011, *MNRAS*, 413, 2173
- Gehrels, N., Barthelmy, S. D., Burrows, D. N., et al. 2008, *ApJ*, 689, 1161
- Ghirlanda, G., Nava, L., Ghisellini, G., et al. 2012, *MNRAS*, 420, 483
- Greiner, J., Bornemann, W., Clemens, C., et al. 2008, *PASP*, 120, 405
- Greiner, J., Krühler, T., Klose, S., et al. 2011, *A&A*, 526, A30
- Guetta, D., Piran, T., & Waxman, E. 2005, *ApJ*, 619, 412
- Guidorzi, C., Vergani, S. D., Sazonov, S., et al. 2007, *A&A*, 474, 793
- Jakobsson, P., Björnsson, G., Fynbo, J. P. U., et al. 2005, *MNRAS*, 362, 245

- Jakobsson, P., Hjorth, J., Fynbo, J. P. U., et al. 2004, *ApJ*, 617, L21
- Jaunsen, A. O., Rol, E., Watson, D. J., et al. 2008, *ApJ*, 681, 453
- Kann, D. A., Klose, S., & Zeh, A. 2006, *ApJ*, 641, 993
- Kann, D. A., Klose, S., Zhang, B., et al. 2011, *ApJ*, 734, 96
- Kann, D. A., Klose, S., Zhang, B., et al. 2010, *ApJ*, 720, 1513
- Kistler, M. D., Yüksel, H., Beacom, J. F., & Stanek, K. Z. 2008, *ApJ*, 673, L119
- Klose, S., Henden, A. A., Greiner, J., et al. 2003, *ApJ*, 592, 1025
- Lü, J., Zou, Y.-C., Lei, W.-H., et al. 2012, *ApJ*, 751, 49
- Langer, N., & Norman, C. A. 2006, *ApJ*, 638, L63
- Levan, A., Fruchter, A., Rhoads, J., et al. 2006, *ApJ*, 647, 471
- Li, L.-X. 2008, *MNRAS*, 388, 1487
- Li, L., Liang, E.-W., Tang, Q.-W., et al. 2012, *ApJ*, 758, 27
- Liang, E.-W., Li, L., Gao, H., et al. 2012, arXiv:1210.5142
- Liang, E.-W., Yi, S.-X., Zhang, J., et al. 2010, *ApJ*, 725, 2209
- Liang, E., & Zhang, B. 2006, *ApJ*, 638, L67
- Lu, R.-J., Wei, J.-J., Qin, S.-F., & Liang, E.-W. 2012, *ApJ*, 745, 168
- Mannucci, F., Salvaterra, R., & Campisi, M. A. 2011, *MNRAS*, 414, 1263
- McBreen, S., Krühler, T., Rau, A., et al. 2010, *A&A*, 516, A71
- Melandri, A., Mundell, C. G., Kobayashi, S., et al. 2008, *ApJ*, 686, 1209
- Nardini, M., Ghisellini, G., Ghirlanda, G., et al. 2006, *A&A*, 451, 821
- Oates, S. R., Page, M. J., Schady, P., et al. 2009, *MNRAS*, 395, 490
- Panaitescu, A., & Vestrand, W. T. 2008, *MNRAS*, 387, 497
- Panaitescu, A., & Vestrand, W. T. 2011, *MNRAS*, 414, 3537
- Pandey, S. B., Swenson, C. A., Perley, D. A., et al. 2010, *ApJ*, 714, 799

- Paul, J., Wei, J., Basa, S., Zhang, S.-N. 2011, *Comptes Rendus Physique*, 12, 298
- Perley, D. A., Bloom, J. S., Klein, C. R., et al. 2010, *MNRAS*, 406, 2473
- Qin, S.-F., Liang, E.-W., Lu, R.-J., Wei, J.-Y., & Zhang, S.-N. 2010, *MNRAS*, 406, 558
- Reichart, D. E., & Price, P. A. 2002, *ApJ*, 565, 174
- Rol, E., Wijers, R. A. M. J., Kouveliotou, C., Kaper, L., & Kaneko, Y. 2005, *ApJ*, 624, 868
- Roming, P. W. A., Koch, T. S., Oates, S. R., et al. 2009, *ApJ*, 690, 163
- Roming, P. W. A., Schady, P., Fox, D. B., et al. 2006, *ApJ*, 652, 1416
- Rykoff, E. S., Aharonian, F., Akerlof, C. W., et al. 2009, *ApJ*, 702, 489
- Sari, R., Piran, T., & Narayan, R. 1998, *ApJ*, 497, L17
- Schady, P., de Pasquale, M., Page, M. J., et al. 2008, *American Institute of Physics Conference Series*, 1000, 200
- Schady, P., Mason, K. O., Page, M. J., et al. 2008, *American Institute of Physics Conference Series*, 1000, 505
- Schady, P., Savaglio, S., Krühler, T., Greiner, J., & Rau, A. 2011, *A&A*, 525, A113
- Schmidt, M. 2001, *ApJ*, 552, 36
- Sokolov, V. V., Fatkhullin, T. A., Castro-Tirado, A. J., et al. 2001, *A&A*, 372, 438
- Starling, R. L. C., Rol, E., van der Horst, A. J., et al. 2009, *MNRAS*, 400, 90
- van Paradijs, J., Groot, P. J., Galama, T., et al. 1997, *Nature*, 386, 686
- Vergani, S. D., Flores, H., Covino, S., et al. 2011, *A&A*, 535, A127
- Vergani, S. D., Molinari, E., Zerbi, F. M., & Chincarini, G. 2004, *A&A*, 415, 171
- Virgili, F. J., Zhang, B., Nagamine, K., & Choi, J.-H. 2011, *MNRAS*, 417, 3025
- Yi, S. X., et al. 2012, *ApJ*, submitted
- Zafar, T., Watson, D., Fynbo, J. P. U., et al. 2011, *A&A*, 532, A143
- Zaninoni, E., Grazia Bernardini, M., Margutti, R., Oates, S., & Chincarini, G. 2013, arXiv:1303.6924

Zhang, B. 2007, *Chin. J. Astro. Astrophys.*, 7, 1

Zhang, B., Dai, X., Lloyd-Ronning, N. M., & Mészáros, P. 2004, *ApJ*, 601, L119

Zheng, W.-K., Deng, J.-S., & Wang, J. 2009, *Research in Astronomy and Astrophysics*, 9, 1103

Table 1. The temporal coverage of the lightcurves, redshifts, spectral indices, apparent magnitudes at selected epochs for 93 GRBs that have well-sampled early optical lightcurves

GRB	$T_{\text{start}}(\text{s})$	$T_{\text{end}}(\text{s})$	z	β_{O}	$M_{\text{R},10^2\text{s}}$	$M_{\text{R},10^3\text{s}}$	$M_{\text{R},1\text{h}}$
990123	22	1229240	1.6	0.75 ± 0.07	10.2	15.4	17.3
021004	155	2421620	2.335	0.39	15.4	16.1	16.5
021211	130	8957	1.01	0.69	14.1	17.8	19.3
030418	288	7192	18.3	16.5	16.8
040924	950	62986	0.859	0.70	17.5	17.7	18.7
041006	230	5577258	0.716	0.55	16.5	17.6	18.2
041219A	441	186558	17.2	16.9
050319	40	994118	3.24	0.74 ± 0.42	16.7	18.1	19.0
050401	3456	1120000	2.9	0.39 ± 0.05	...	19.9	20.9
050408	3352	36710070	1.2357	0.28 ± 0.33	18.3	19.6	20.3
050502A	47	17850	3.793	0.76 ± 0.16	13.9	17.0	18.3
050525A	66	35638	0.606	0.97 ± 0.10	14.2	16.1	17.8
050721	1484	248596	...	1.16 ± 0.35	...	16.8	18.6
050730	67	72697	3.969	0.52 ± 0.05	15.9	16.7	17.3
050801	24	21652	1.56	1.00 ± 0.16	14.7	16.7	18.1
050820A	230	663300	2.612	0.72 ± 0.03	16.5	15.2	16.7
050824	635	8994457	0.83	0.40 ± 0.04	17.1	18.5	19.2
050922C	745	606010	2.198	0.51 ± 0.05	14.9	15.9	16.9
051021	1611	35820	...	0.75	17.5	18.2	18.6
051109A	40	1040000	2.346	0.70	14.9	16.6	17.7
051111	32	7588	1.55	0.76 ± 0.07	13.7	15.7	17.2
060110	25	4781	...	0.75	12.9	14.8	15.9
060111B	30	264806	...	0.70	16.2	19.0	20.6
060124	3335	1980000	2.296	0.73 ± 0.08	...	15.4	16.7
060206	319	201580	4.048	0.73 ± 0.05	15.5	17.9	19.7
060210	63	7190	3.91	0.37	17.8	18.1	19.7
060218	253	2850000	0.0331	0.75	21.0	20.1	19.6
060418	76	7659	1.489	0.78 ± 0.09	13.9	15.7	17.4
060512	112	5927	0.4428	0.68 ± 0.05	15.4	17.2	18.2
060526	60	893550	3.21	0.51 ± 0.32	15.0	16.5	17.3
060605	74	6317	3.78	1.06	15.9	15.6	17.1

Table 1—Continued

GRB	$T_{\text{start}}(\text{s})$	$T_{\text{end}}(\text{s})$	z	β_{O}	$M_{\text{R},10^2\text{s}}$	$M_{\text{R},10^3\text{s}}$	$M_{\text{R},1\text{h}}$
060607A	73	14733	3.082	0.72 ± 0.27	15.9	17.0	19.0
060614	1547	1276350	0.125	0.47 ± 0.04	20.9	20.1	19.6
060729	696	662390	0.54	0.78 ± 0.03	15.3	15.6	15.8
060904B	21	163131	0.703	1.11 ± 0.10	16.8	16.4	18.9
060906	661	13610	3.686	0.56 ± 0.02	20.1	18.8	19.8
060908	825	7242	2.43	0.30	14.7	17.5	19.0
060912A	1100	23900	0.937	0.62	...	18.0	19.3
060926	57	1200	3.2	0.82 ± 0.01	16.7	19.1	...
060927	17	1169	5.6	0.86 ± 0.03	16.0	16.6	18.2
061007	30	14599	1.261	0.78 ± 0.02	9.6	13.4	15.7
061121	49	554	1.1588	0.95	11.6	12.6	14.1
061126	36	156381	1.1588	0.95	13.8	17.3	18.5
070110	662	34762	1.547	0.55 ± 0.04	18.6	19.0	19.2
070208	329	13460	1.165	0.68	18.6	19.8	20.4
070311	74	350926	...	1.00 ± 0.20	14.8	16.6	17.6
070318	61	87366	0.836	0.78	15.5	15.4	17.0
070411	184	516628	2.954	0.75	16.5	16.6	18.1
070419A	206	62218	0.97	0.80	20.4	18.8	20.5
070420	116	10842	...	0.75	15.6	16.2	17.4
070518	1069	311763	1.16	0.80	18.0	19.6	20.6
070611	274	8867	2.04	0.73	17.7	20.1	18.6
071003	569	5003	1.605	1.25 ± 0.09	13.4	17.3	18.7
071010A	321	523226	0.98	0.68	17.0	16.7	17.7
071010B	64	174464	0.947	0.00	16.8	17.2	18.0
071025	175	14885	...	0.42 ± 0.08	17.7	16.2	17.5
071031	287	350926	2.692	0.64 ± 0.01	19.5	18.1	18.8
071112C	132	69638	0.823	0.63 ± 0.29	17.5	18.1	19.3
071122	1303	9047	1.14	0.83	...	20.1	19.8
080310	151	124416	2.4266	0.42 ± 0.12	17.3	16.9	17.5
080319A	150	4462	...	0.77 ± 0.02	21.0	20.3	21.2
080319B	5	4590000	0.937	0.75	9.4	14.1	16.0

Table 1—Continued

GRB	$T_{\text{start}}(\text{s})$	$T_{\text{end}}(\text{s})$	z	β_{O}	$M_{\text{R},10^2\text{s}}$	$M_{\text{R},10^3\text{s}}$	$M_{\text{R},1\text{h}}$
080319C	78	1432	1.949	0.77 ± 0.02	16.8	17.4	18.7
080330	89	116557	1.51	0.49	17.8	17.5	18.3
080413A	7	18339	2.433	0.67	14.1	16.5	18.2
080413B	77	5185072	1.1	0.25 ± 0.07	16.2	18.1	18.9
080506	210	5371	...	0.95 ± 0.05	16.4	17.6	18.5
080603A	105	350436	...	0.75	21.5	18.4	18.5
080710	417	34762	0.845	0.80 ± 0.09	19.1	16.9	16.7
080804	1160	26112	2.2	0.43	...	17.9	19.2
080810	38	7898	3.35	0.44	12.6	14.7	16.4
080913	576	870036	6.7	0.79 ± 0.03	19.3	21.7	23.1
080928	390	13425	1.692	1.08 ± 0.02	18.7	17.0	17.2
081008	109	184525	1.692	1.08 ± 0.02	17.0	17.4	18.7
081029	529	252674	3.85	0.00	15.6	17.4	18.0
081109A	169	66600	...	0.75	17.8	18.1	19.3
081126	102	541	...	0.75	15.4	15.5	16.1
081203A	78	5758	2.1	0.60	14.0	13.1	15.2
090102	41	264553	1.547	0.74	14.2	18.1	19.7
090313	205	7874700	3.375	0.71	18.8	15.8	16.8
090426	86	10748	2.609	0.76 ± 0.14	16.4	18.6	19.8
090510	114	103794	0.903	0.76 ± 0.14	22.2	21.5	21.9
090618	76	72576	0.54	0.50	13.7	15.5	16.4
090726	204	3015	2.71	0.75	19.1	20.7	...
090812	27	142	2.452	0.36	15.1	18.5	20.4
100219A	936	34978	0.49	0.18	16.4	19.0	20.8
100418A	1099	1371570	...	0.75	...	21.4	20.5
100728B	159	5644	...	0.75	16.3	18.8	19.7
100901A	634	543008	1.408	0.75	22.2	17.6	18.2
100906A	51	10937	1.408	0.75	13.0	14.9	16.4
101024A	219	160000	...	0.75	...	19.3	19.8
110205A	540	384000	...	0.75	...	14.2	16.1
110213A	104	183368	...	0.75	15.1	14.4	14.8

Table 2. The temporal coverage of the lightcurves, redshifts, spectral indices, peak time, apparent magnitudes at selected epochs for 39 GRBs that have an onset bump in their optical lightcurves

GRB	z	$T_{\text{start}}(\text{s})$	$T_{\text{end}}(\text{s})$	$t_{\text{p}}(\text{s})$	$M_{\text{R},10^2\text{s}}$	$M_{\text{R},10^3\text{s}}$	$M_{\text{R},1\text{h}}$	$M_{\text{R},t_{\text{p}}}$
030418	...	288	7192	1190	18.3	16.5	16.8	16.4
050502A	3.793	47	17850	58	13.9	17.1	19.0	13.4
050820A	2.612	230	663300	477	16.5	15.2	16.7	14.6
060110	...	25	4781	50	12.9	14.8	15.9	12.5
060111B	...	30	264806	54	16.2	19.0	20.6	15.7
060418	1.489	76	7659	170	13.9	15.7	17.4	13.4
060605	3.78	74	6317	590	16.1	15.7	17.5	15.4
060607A	3.082	73	14733	179	15.9	17.0	19.0	14.7
060904B	0.703	21	163131	85	17.2	16.3
060906	3.686	661	13610	1149	20.1	18.8	20.0	18.8
061007	1.261	30	14599	77	9.6	13.4	15.7	9.5
061121	1.1588	49	554	208	11.7	12.6	14.1	11.0
070318	0.836	61	87366	507	15.5	15.4	17.0	14.7
070419A	0.97	206	62218	765	20.4	18.8	20.5	18.6
070420	...	116	10842	202	15.6	16.2	17.4	14.8
071010A	0.98	321	523226	586	19.3	17.1	18.7	16.7
071010B	0.947	64	174464	287	16.8	17.2	18.0	16.6
071025	...	175	14885	548	17.7	16.2	17.7	15.8
071031	2.692	287	350926	1213	19.5	18.1	18.8	18.1
071112C	0.823	132	69638	178	17.5	18.1	19.3	16.7
080310	2.4266	298	124416	184	17.8	19.0	20.6	17.0
080319A	...	151	4462	238	21.0	20.3	21.2	19.6
080330	1.51	89	116557	578	17.8	17.9	19.4	17.5
080413A	2.433	7	18339	150	14.5	16.5	18.2	14.3
080603A	...	105	350436	1044	21.5	18.4	18.5	18.3
080710	0.845	417	34762	1934	21.1	17.2	17.0	16.7
080810	3.35	38	7898	117	12.6	14.7	16.4	12.6
080928	1.692	390	13425	2290	18.7	17.0	17.4	16.7
081008	1.692	109	184525	163	17.0	17.4	18.7	15.7
081109A	...	169	66600	559	17.8	18.1	19.3	17.7
081126	...	102	541	159	15.4	15.5	16.1	15.0
081203A	2.1	78	5758	295	14.0	13.1	15.2	12.3
090102	1.547	41	264553	50	14.2	18.1	20.3	13.3
090313	3.375	205	7874700	1315	18.8	15.8	16.8	15.6
090510	0.903	114	103794	1579	22.2	21.5	21.9	21.5
090726	2.71	204	3015	290	19.2	18.0
090812	2.452	27	142	71	15.1	18.5	20.4	14.8

Table 2—Continued

GRB	z	$T_{\text{start}}(\text{s})$	$T_{\text{end}}(\text{s})$	$t_{\text{p}}(\text{s})$	$M_{\text{R},10^2\text{s}}$	$M_{\text{R},10^3\text{s}}$	$M_{\text{R},1\text{h}}$	$M_{\text{R},t_{\text{p}}}$
100901A	1.408	634	543008	1260	22.2	17.6	18.2	17.3
100906A	1.408	51	10937	101	13.0	14.9	16.4	13.0
110205A	...	540	384000	948	...	14.2	16.1	14.2
110213A	...	104	183368	294	15.1	14.6	15.8	13.6

Table 3. The temporal coverage of the lightcurves, redshifts, spectral indices, peak time, apparent magnitudes at selected epoches for 26 GRBs that have an early shallow decay segment in their optical lightcurves

GRB	z	$T_{\text{start}}(\text{s})$	$T_{\text{end}}(\text{s})$	$T_{\text{p}}(\text{s})$	$M_{\text{R},10^2\text{s}}$	$M_{\text{R},10^3\text{s}}$	$M_{\text{R},1\text{h}}$	$M_{\text{R},t_{\text{b}}}$
021004	2.335	156	2421620	9909	15.4	16.1	16.5	17.1
040924	0.859	950	62986	1722	17.5	17.7	18.7	17.9
041006	0.716	230	5580000	11346	16.5	17.6	18.2	18.9
050319	3.24	40	994118	535	17.3	19.3	22.2	18.1
050408	1.2357	3352	3670000	40389	18.3	19.6	20.3	22.0
050730	3.969	67	72697	11362	15.9	16.7	17.3	18.3
050801	1.56	24	21652	1512	16.2	16.9	18.1	17.2
050922C	2.198	745	606010	4083	14.9	15.9	16.9	17.0
051021	...	1611	35820	4932	17.5	18.2	18.6	18.8
051109A	2.346	40	1040000	445	14.9	16.6	17.8	16.0
060111B	...	30	13700000	36	19.5	13.9
060210	3.91	63	7190	958	17.8	18.3	19.7	18.2
060526	3.21	60	893550	20940	15.0	16.5	17.3	18.9
060605	3.78	74	6317	23275	17.7	18.2	18.4	19.0
060729	0.54	696	662390	4131	15.3	15.6	15.9	16.1
060927	5.6	17	1169	37	16.1	21.6	24.6	14.2
061126	1.1588	36	156381	14809	17.1	18.1	18.7	19.6
070110	1.547	662	34762	14290	18.6	19.0	19.2	19.7
070208	1.165	1166	4854	12732	18.6	19.8	20.4	21.3
070411	2.954	183	516628	108994	16.9	18.2	18.9	21.4
070518	1.16	2113	311763	30000	18.0	19.6	20.6	22.7
071010A	0.98	321	523226	12528	17.1	17.8	18.2	18.9
080413A	2.433	7	18339	73	15.4	14.0
081029	3.85	529	252674	2323	15.6	17.4	20.0	18.9
090426	2.609	86	10748	257	16.5	19.2	21.6	17.5
090618	0.54	76	72576	31120	14.0	15.6	16.4	18.3

Table 4. Extinction of the GRB host galaxies (A_V^{host}) collected from the literature

GRB	A_V	Ref.	GRB	A_V	Ref.	GRB	A_V	Ref.
970228	0.50	(1)	050820A	0.07 ± 0.01	(7)	070419A	0.42 ± 0.37	(3)
971214	0.43 ± 0.08	(1)	050824	0.15 ± 0.03	(8)	070518	0.30	(3)
980425	1.90 ± 0.10	(2)	050904	1.00	(10)	071003	0.34 ± 0.11	(3)
980613	0.45	(-)	051028	0.70	(11)	071010A	0.64 ± 0.09	(3)
980703	1.50 ± 0.11	(1)	051111	0.20 ± 0.10	(-)	071025	1.09 ± 0.20	(18)
990510	0.22 ± 0.07	(3)	060111B	3.60 ± 0.50	(12)	071031	0.14 ± 0.13	(3)
990712	0.50 ± 0.10	(2)	060124	0.05 ± 0.26	(3)	071112C	0.23 ± 0.21	(3)
991208	0.05	(4)	060206	0.01 ± 0.02	(12)	080310	0.19 ± 0.05	(3)
000301C	0.09 ± 0.04	(1)	060210	1.18 ± 0.10	(3)	080319C	0.59 ± 0.12	(3)
000418	0.96	(1)	060418	0.12 ± 0.05	(2)	080330	0.19 ± 0.08	(3)
000926	0.18 ± 0.06	(1)	060526	0.05 ± 0.11	(-)	080413A	0.13 ± 0.07	(3)
020813	0.14 ± 0.04	(1)	060614	0.11 ± 0.03	(8)	080710	0.11 ± 0.04	(3)
021004	0.30	(1)	060729	0.07 ± 0.02	(7)	080721	0.60	(19)
030226	0.53	(1)	060904B	0.08 ± 0.08	(8)	080810	0.16 ± 0.02	(3)
030323	0.13 ± 0.09	(3)	060906	0.09	(3)	080913	$(0.58) \pm 0.67$	(3)
030328	0.05 ± 0.15	(5)	060908	0.05 ± 0.03	(7)	080928	0.29 ± 0.03	(3)
030329	0.30 ± 0.03	(1)	060912A	0.46 ± 0.23	(14)	081008	0.29 ± 0.03	(8)
030429	0.34	(1)	060926	0.32 ± 0.02	(8)	081203A	0.09 ± 0.04	(3)
030723	0.32 ± 0.22	(5)	060927	0.12	(8)	090102	0.12 ± 0.11	(3)
041219A	6.80 ± 1.60	(6)	061007	0.39 ± 0.01	(8)	090313	0.34 ± 0.15	(3)
050319	0.05 ± 0.09	(7)	061126	0.10 ± 0.06	(3)	090323	0.14 ± 0.00	(3)
050401	0.65 ± 0.04	(8)	070110	0.11 ± 0.04	(3)	090328	0.22 ± 0.06	(20)
050408	0.73 ± 0.18	(9)	070125	0.11 ± 0.04	(15)	090618	0.30 ± 0.10	(21)
050416A	0.70 ± 0.70	(2)	070306	5.45 ± 0.61	(16)	090902B	0.20 ± 0.06	(22)
050525A	0.25 ± 0.16	(1)	070311	0.80 ± 0.15	(17)	090926A	0.13 ± 0.06	(3)
050730	0.12 ± 0.02	(8)	070318	0.44 ± 0.11	(14)	091127	0.20	(23)
050801	0.30 ± 0.18	(2)						

References. — (1) Liang & Zhang (2006); (2) Mannucci et al.(2011); (3) Kann et al.(2010); (4) Sokolov et al.(2001);(5) Kann et al.(2006); (6) Gotz, D. et al (2011) (7) de Ugarte Postigo et al.(2011); (8) Zafar et al.(2011); (9) de Ugarte Postigo et al.(2007); (10) Berger et al.(2007); (11) Castro-Tirado (2006); (12) Fynbo et al.(2009); (13) Ferrero et al.(2009); (14) Schady et al.(2011); (15) Schady et al.(2008); (16) Jaunsen et al.(2008); (17) Guidorzi et al.(2007); (18) Perley et al.(2009); (19) Starling et al.(2009); (20) McBreen (2010); (21) Cano et al.(2011); (22) Pandey et al.(2010); (23) Vergani et al.(2011).

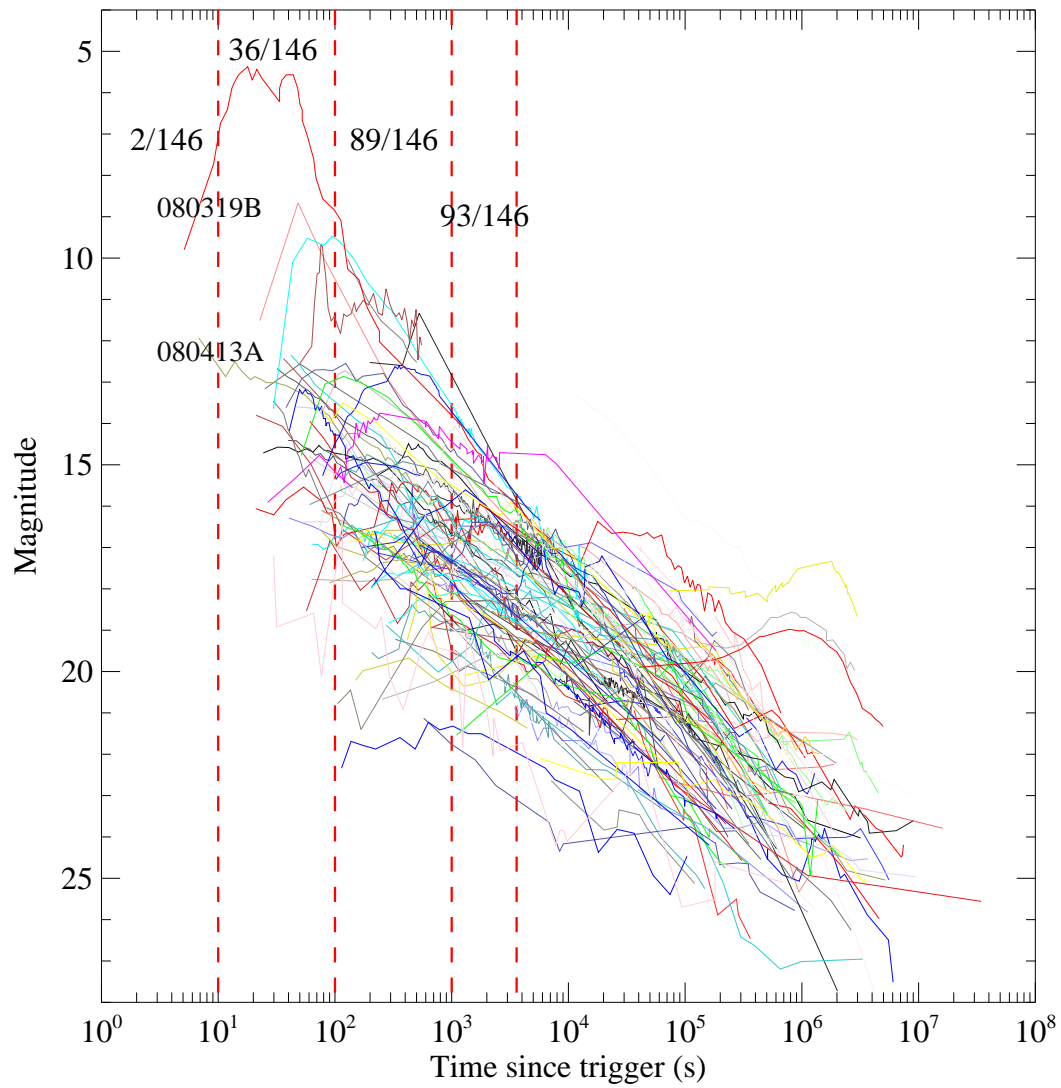


Fig. 1.— Galactic extinction corrected R band lightcurves of 146 GRBs. Different colors are used to make it easier to discern different GRBs. The detection fractions at different epochs are marked.

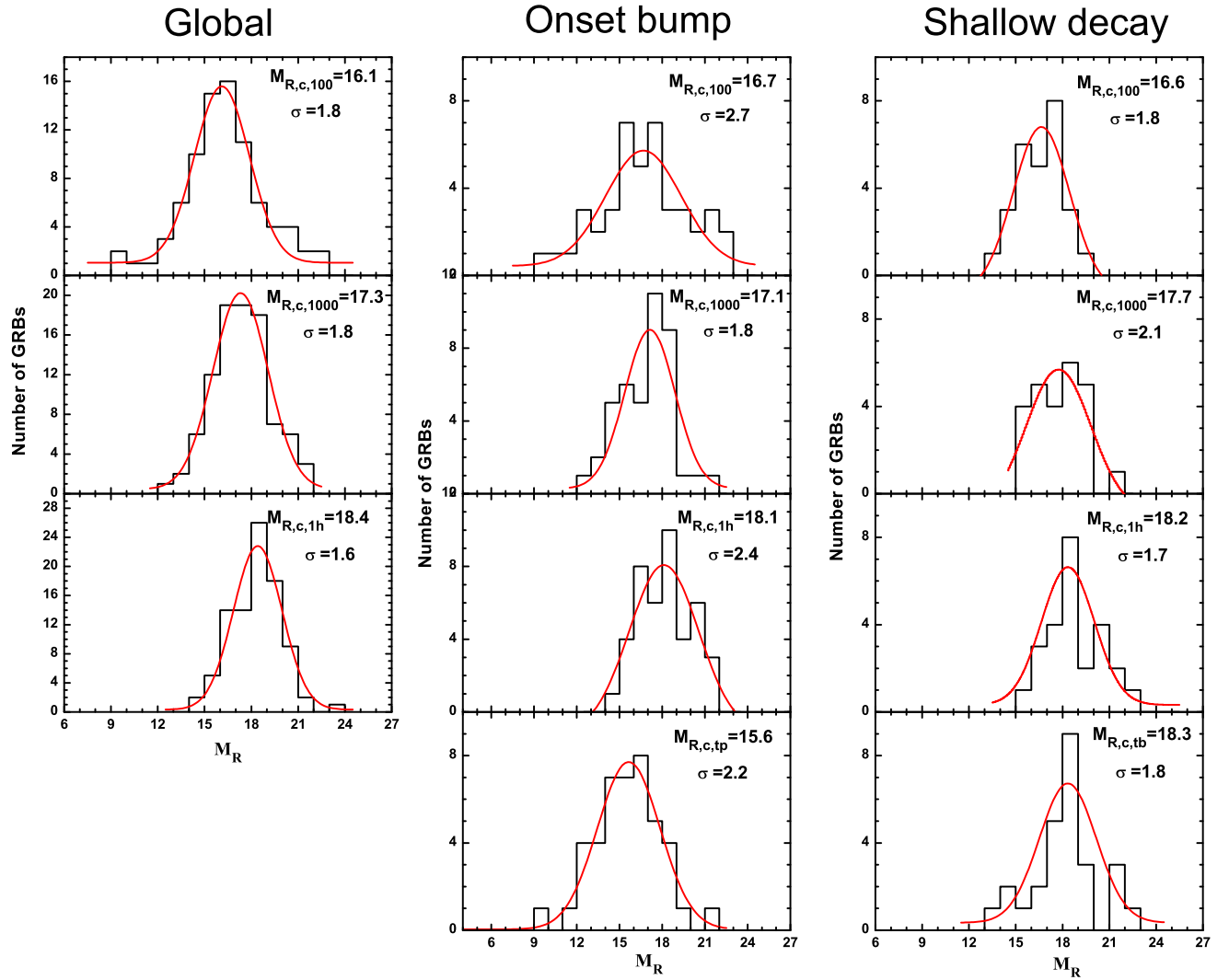


Fig. 2.— R band magnitude distributions with Gaussian fits at different epochs for the full sample (left panels), the onset bump sample (middle panels), and the shallow decay segment sample (right panels). The central values of the Gaussian fits are also marked.

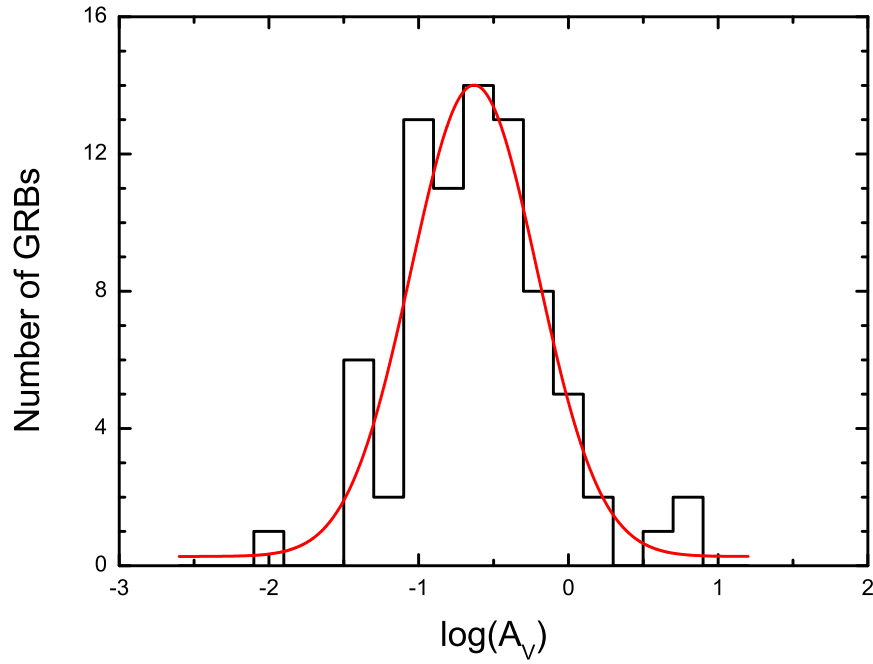


Fig. 3.— Distribution of $\log A_V$ values along with our best fit with a Gaussian function for 79 GRBs collected from the literature. The Gaussian fit gives $\log(A_V) = -0.63 \pm 0.42(1\sigma)$.

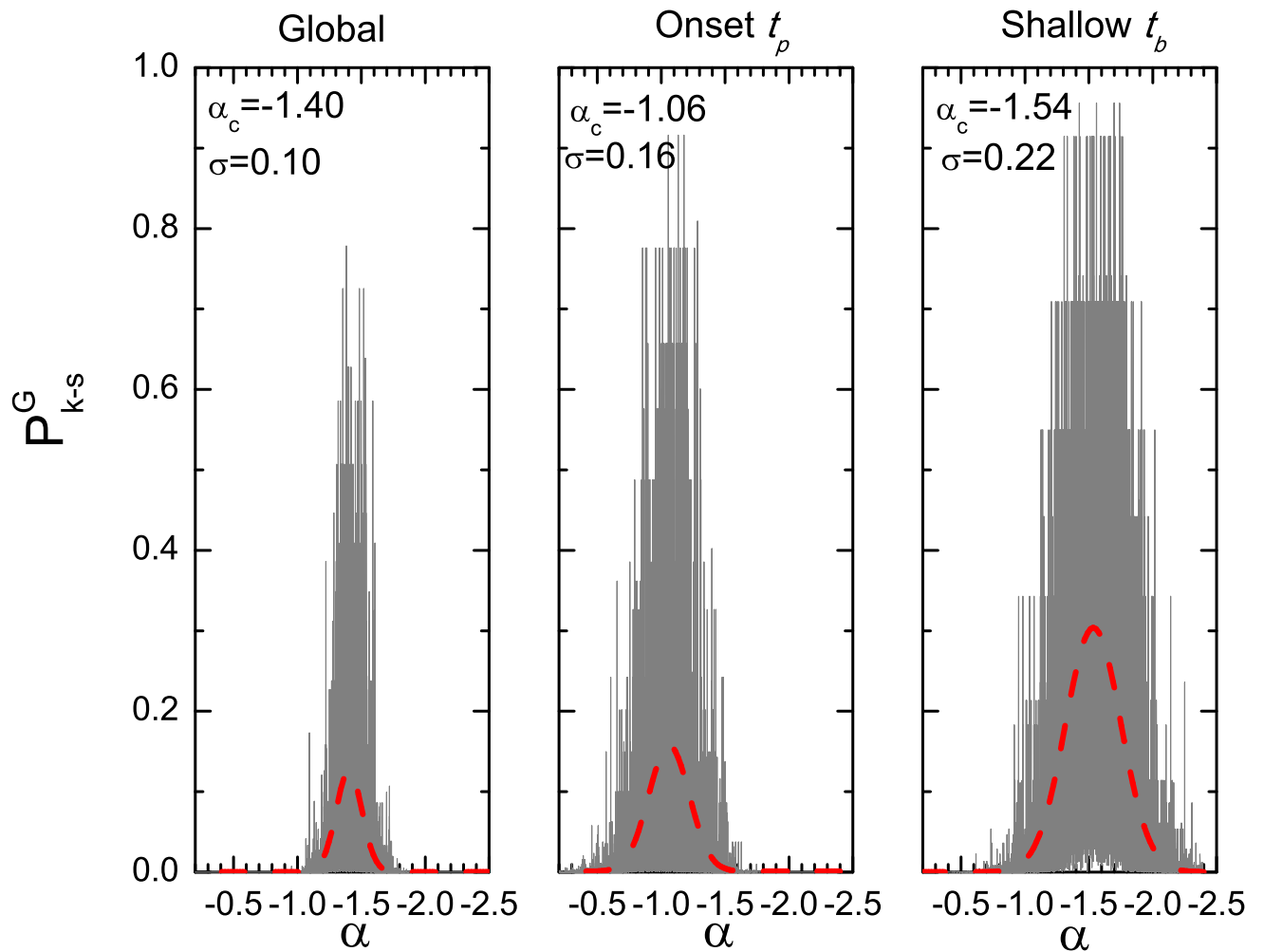


Fig. 4.— Distributions of the K-S test probability P_{K-S}^G of the power-law indices of the optical luminosity functions for the full sample at $t = 10^3$ seconds (panel a), for the onset bump sample at t_p (panel b), and for the shallow decay segment sample at t_b (panel c). The dashed curves are Gaussian fits to the distributions of the average P_{K-S}^G in each bin. The central values of the Gaussian fits are also marked.

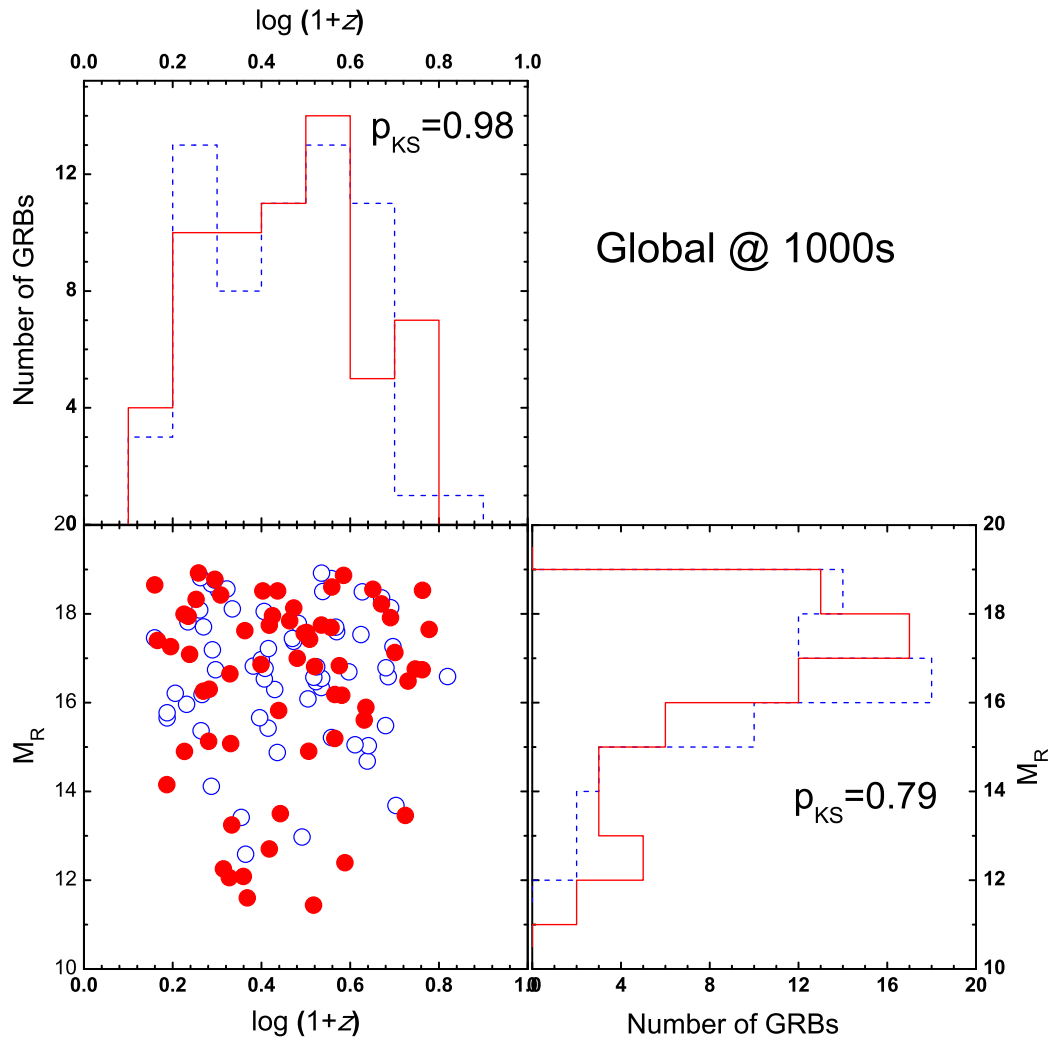


Fig. 5.— Illustration of the best consistency between the observations (open dots and dashed lines) and our simulations with an optical luminosity function $\Phi \propto L^{-1.40 \pm 0.10}$ (solid dots and solid lines) for the full sample at $t = 10^3$ s in two-dimensional $\log M_R - \log(1+z)$ distributions and one-dimensional $\log(1+z)$ and M_R distributions.

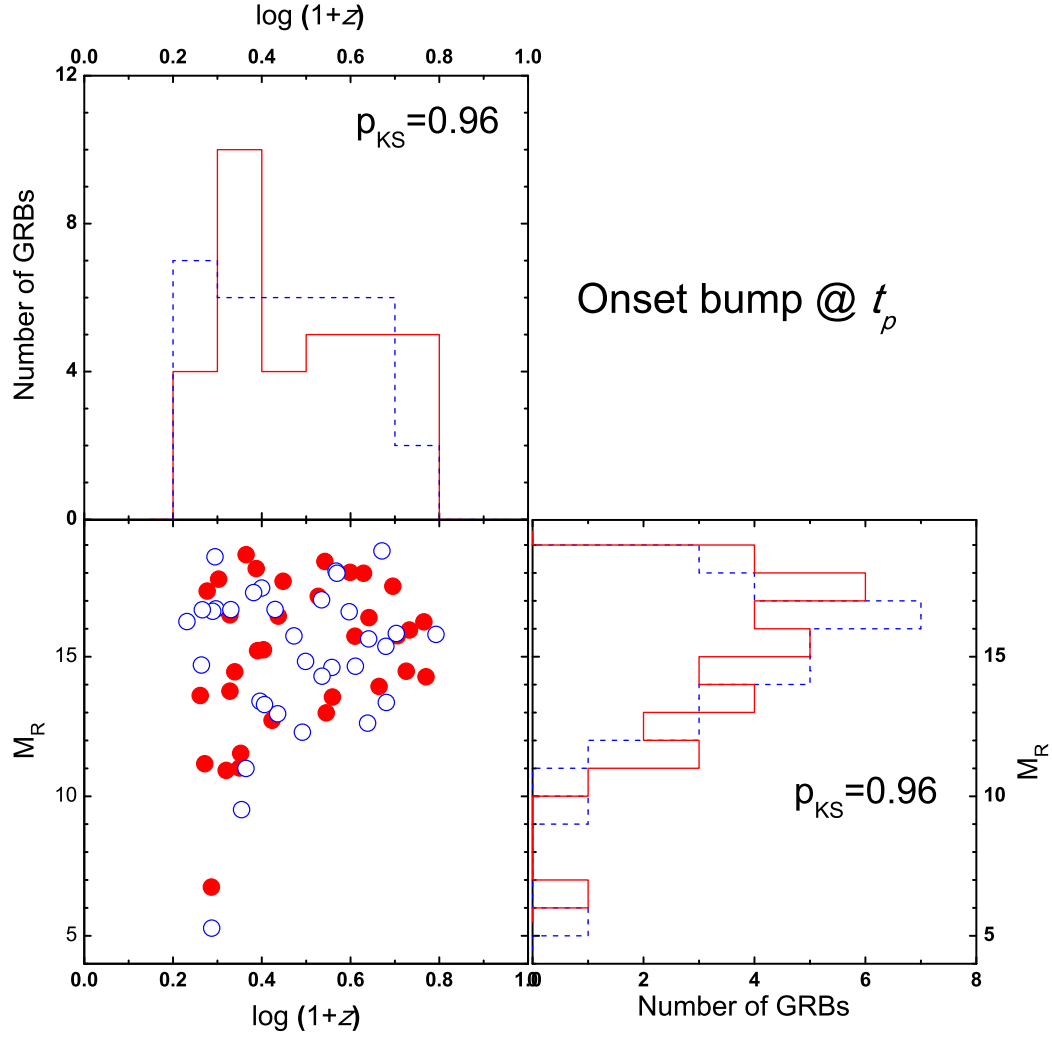


Fig. 6.— Same as Fig. 5, but for the onset bump sample at t_p with a luminosity function $\Phi \propto L^{-1.06 \pm 0.16}$.

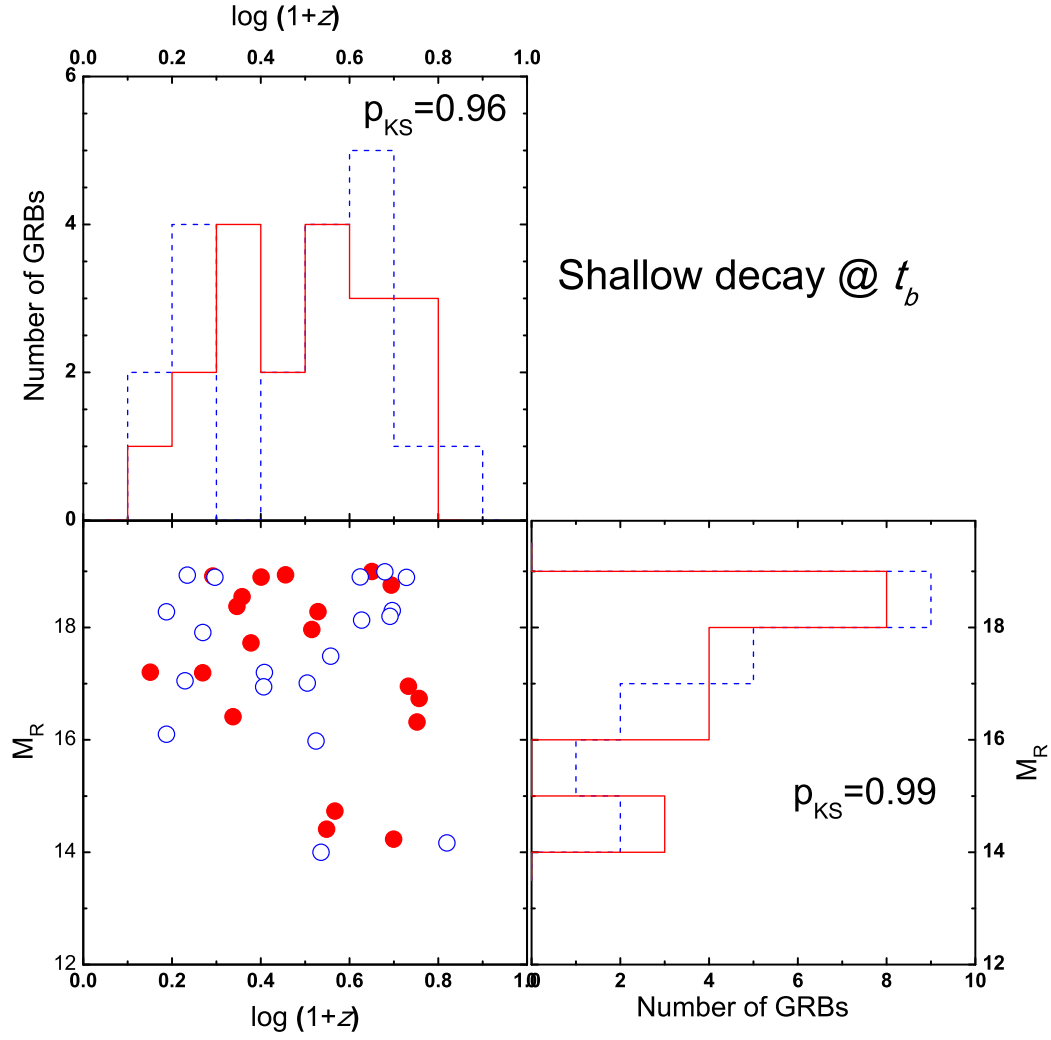


Fig. 7.— Same as Fig. 5, but for the shallow decay segment at t_b with a luminosity function $\Phi \propto L^{-1.54 \pm 0.22}$.

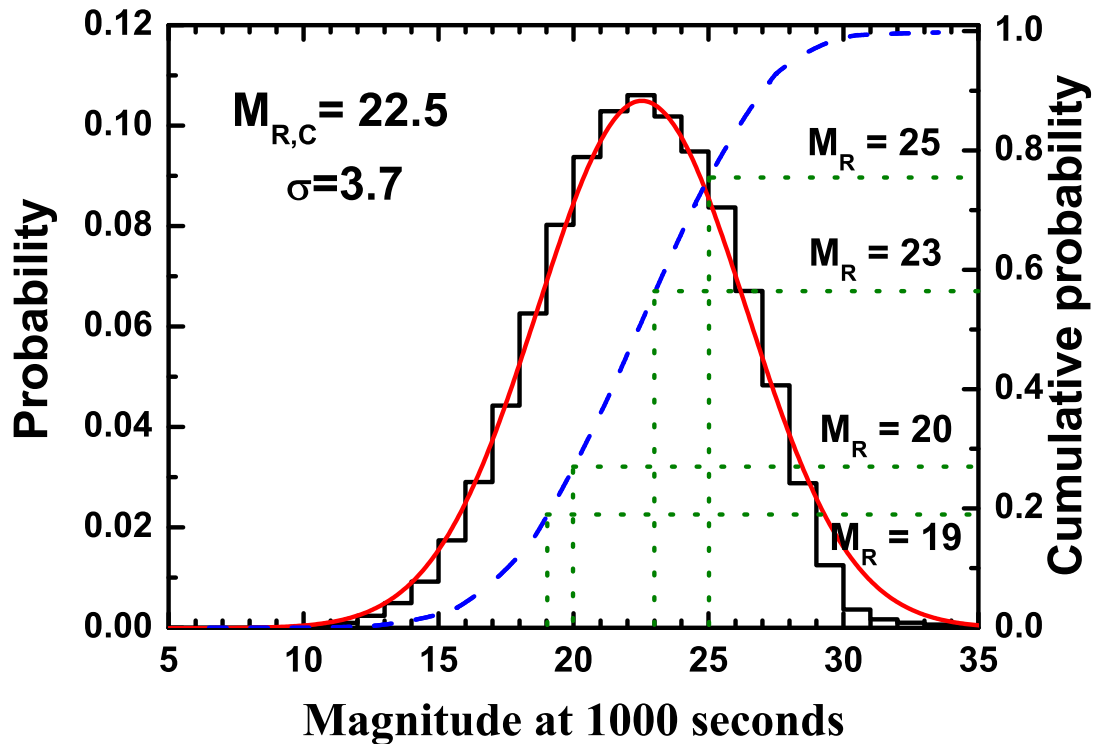


Fig. 8.— The observer-frame probability distributions of the apparent R band magnitude at $t = 10^3$ seconds (histogram) along with the Gaussian fit (smooth curve). The cumulative probability distribution is also shown with a dashed line. The peak of the probability distribution is $M_{R,c} = 22.5$ mag. The dotted lines mark the probabilities of the optical afterglow detection at the instrument thresholds $M_R = 19$ and $M_R = 23$, which correspond to small robotic telescopes and the VT onboard the future mission SVOM.